Formic Acid Convenient Liquid Hydrogen Storage for Mobile Applications

H. Junge, B. Loges, A. Boddien, M. Beller

This document appeared in

Detlef Stolten, Thomas Grube (Eds.):
18th World Hydrogen Energy Conference 2010 - WHEC 2010
Parallel Sessions Book 4: Storage Systems / Policy Perspectives, Initiatives and Co-operations
Proceedings of the WHEC, May 16.-21. 2010, Essen
Schriften des Forschungszentrums Jülich / Energy & Environment, Vol. 78-4
Institute of Energy Research - Fuel Cells (IEF-3)
Forschungszentrum Jülich GmbH, Zentralbibliothek, Verlag, 2010
ISBN: 978-3-89336-654-5

Graphitic Nanofibres as Catalyst for Improving the Dehydrogenation Behavior of Complex Aluminium Hydrides

M. Sterlin Leo Hudson, Himanshu Raghubanshi, D. Pukazhselvan, O.N. Srivastava*, Hydrogen Energy Center, Department of Physics, Banaras Hindu University, Varnasi, India

Abstract

In the present work, we explored the catalytic effect of graphitic nanofibres (GNF) particularly of two different morphology, namely planar graphitic nanofibre (PGNF) and helical graphitic nanofibre (HGNF) for enhancement of hydrogen desorption from complex aluminium hydrides such as $LiAlH_4$ and $LiMg(AlH_4)_3$. We found that the catalytic activity of fibres depends mainly on its morphology. Hence helical morphology fibres possess superior catalytic activity than planar graphitic nanofibres. The desorption temperature for 8 mol% HGNF admixed $LiAlH_4$ gets lowered from 159°C to 128°C with significantly faster kinetics. In 8 mol% HGNF admixed $LiMg(AlH_4)_3$ sample, the desorption temperature gets lowered from 105°C to ~70°C. The activation energy calculated for the first step decomposition of $LiAlH_4$ admixed with 8 mol% HGNF is ~68 $kJmol^{-1}$, whereas that for pristine $LiAlH_4$ it is 107 kJ/mol. The activation energy calculated for as synthesized $LiMg(AlH_4)_3$ is ~66 kJ/mol. Since the first step decomposition of $LiMg(AlH_4)_3$ occurs during GNF admixing, the activation energy for initial step decomposition of GNF admixed $LiMg(AlH_4)_3$ could not be estimated.

1 Introduction

The growing interest on finding effective catalyst for improving the dehydrogenation/re-hydrogenation behavior of complex metal hydrides after the pioneering work of Bogdanovic et al [1] on the reversibility of $NaAlH_4$ triggers research on various catalysts including transition and rare earth metal based catalysts. Aluminium hydrides, $LiAlH_4$ and $LiMg(AlH_4)_3$ possess quite high gravimetric hydrogen capacity of 10.6 and 9.7 wt.%H_2, respectively. The fast desorption of hydrogen from these compounds becomes feasible with the use of a suitable catalysts. There is an ongoing search for finding an effective catalyst for improving the dehydrogenation/re-hydrogenation behavior of complex hydrides [2]. Recent studies by Berseth et al [3] reveal that carbon nano-variants are found to possess catalytic effect on complex hydrides. Among the carbon nanovariants, graphitic nanofibres are very promising due to their large number of localized σ bond electrons around the edges of parallel graphitic sheets, which provides more catalytically active sites [4, 5]. Advantageous features of carbon nanofibre are that it is light weight, not prone to oxidation nor gets substituted in the alanate lattice. In the light of above, we explored the use of graphitic nanofibres of two different morphology namely planar graphitic nanofibre (PGNF) and helical graphitic nanofibre

* Corresponding author: Email: hepons@yahoo.com

(HGNF) for possible improvement in dehydrogenation characteristics of $LiMg(AlH_4)_3$ and $LiAlH_4$. The catalytic activity of GNFs has been proven for binary hydride, MgH_2 [6]. The optimum concentration of GNFs on $LiAlH_4/LiMg(AlH_4)_3$ for the present study has been found to be 8 mol%. Our present investigation reveals that HGNFs possess superior catalytic activity than PGNFs.

The motivation behind our present investigation is to show the catalytic activity of HGNF on $LiMg(AlH_4)_3$ and $LiAlH_4$ for reducing the decomposition temperature and increasing the dehydrogenation kinetics, and hence we deduce the activation energy for initial decomposition reaction, which is comparable to that obtained by using known transition metal based catalysts (e.g. $TiCl_3$, VCl_3 etc.). We found that admixing HGNF greatly improves the desorption kinetics and decreases the decomposition temperature of both $LiMg(AlH_4)_3$ and $LiAlH_4$.

2 Experimental Method

As received $LiAlH_4$ (Aldrich, 95%) and $MgCl_2$ (Alfa Aesar, 99%) have been used without further purification. $LiAlH_4$ and $MgCl_2$ in the molar ratio 3:1 was ball-milled together with two steel balls of 12.5 mm each and one ball with 4 mm in a chrome-nickel stainless steel milling vial under argon atmosphere in a locally fabricated attritor ball-miller with ball-to-powder mass ratio 10:1. The expected reaction $3LiAlH_4 + MgCl_2 \rightarrow LiMg(AlH_4)_3 + 2LiCl$ has been found to get completed in one hour of ball-milling. All operations on the samples were done under dry argon atmosphere in a glove box to prevent reaction with moisture and oxygen in the air. The graphitic nanofibres are being synthesized in our laboratory through dissociation of hydrocarbon (acetylene/ethylene) over Ni/Fe nanoparticles catalyst in an open furnace at 650°C under flowing He and H_2 gas both with an optimized flow rate of 1500 sccm. In keeping with the known results [7, 8], we have found that morphology of GNF is dependent on the shape of the Ni/Fe nanoparticles. Whereas for faceted Ni/Fe nanoparticles helical GNF get formed and for non-faceted Ni/Fe nanoparticles, planar GNF are found to grow. Thermal decompositions of GNF admixed $LiAlH_4$ and $LiMg(AlH_4)_3$ samples were monitored using computerized pressure composition isotherm (P-C-I) measurement system supplied by Advanced Materials Corporation.

Structural characterization of the samples was carried out through XRD, Philips PW-1710 and X'Pert PRO (PANalytical) X-ray diffractometer equipped with graphite monochromator employing CuK_α radiation (λ= 1.5402Å). Exposure of the sample to atmosphere has been avoided by covering the XRD holder by fine layer of Parafilm (Pechiney plastic packing). The microstructural characterization has been done through Transmission electron Microscope (Technai, 200 kV).

3 Results and Discussions

3.1 Lithium-magnesium alanate

$LiMg(AlH_4)_3$ has been synthesized mechano-chemically through the following reaction

$$3Li(AlH_4)_3 + MgCl_2 \rightarrow LiMg(AlH_4)_3 + 2LiCl \quad (1)$$

by using a locally fabricated attritor ball-miller. The above reaction gets completed in ~1 hour of ball-milling, which gets confirmed from the X-ray diffractogram, a representative XRD profile is shown in Figure 1(a). Since peaks corresponding only to the reaction product were present in the XRD profile, it becomes evident that complete conversion of the above said chemical reaction (eq. (1)) has taken place. Figure 1(b) shows the XRD of purified (through acid treatment) helical GNF used as catalyst for our present study.

Following the known results [9], the thermal decomposition behavior of $LiMg(AlH_4)_3$ can be described as follows,

$$LiMg(AlH_4)_3 \rightarrow LiMgAlH_6 + 2Al + 3H_2 \quad (\sim 100^\circ C) \quad (2)$$

$$LiMgAlH_6 \rightarrow LiH + MgH_2 + Al + 3/2H_2 \quad (\sim 150^\circ C) \quad (3)$$

$$2MgH_2 + 3Al \rightarrow Al_3Mg_2 + 2H_2 \quad (\sim 340^\circ C) \quad (4)$$

The temperature programmed desorption (TPD) curve was monitored from room temperature to 240°C at the heating rate of 1°C/min. It has been observed from the TPD profile that the peak decomposition temperature of Eq. (2) is 105.5°C and that of Eq. (3) is 149.6°C. For 8 mol% HGNF admixed $LiMg(AlH_4)_3$, Eq. (2) occurs at the time of catalyst admixing. However, for the heating rate of 1°C/min, the peak desorption temperature for 8 mol% HGNF admixed $LiMg(AlH_4)_3$ corresponds to Eq. (3) has been lowered from 149.6°C to 127.9°C**.** A representative TPD curve is shown in Figures 2(a) and 2(b).

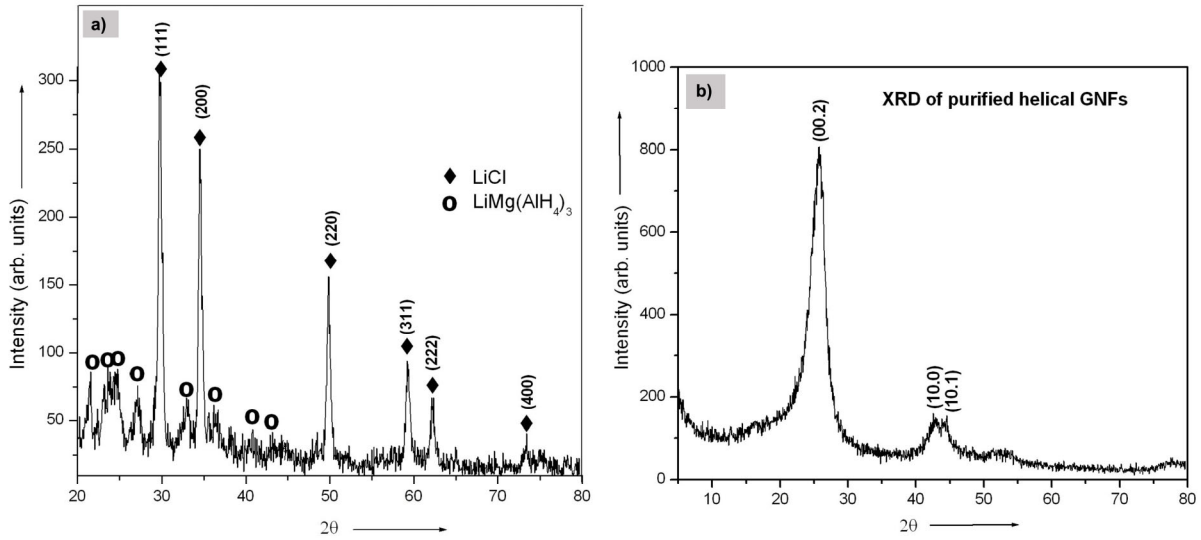

Figure 1: X-ray diffractorgram of a) as synthesized $LiMg(AlH_4)_3$ + 2LiCl mixture and b) purified GNFs used as catalyst.

The LiCl in the reaction product acts as a dead weight and it does not take part in the above mentioned reactions. Purification of LiCl from $LiMg(AlH_4)_3$ + 2LiCl mixture is a tedious and time consuming process which may also leads to the decomposition of $LiMg(AlH_4)_3$. Therefore purification may not be of help for practical applications [10]. In order to calculate

the rate constant of reaction and hence to calculate the activation energy, a comparative study without considering the dead weight of LiCl has been made. A representative TPD curve of $LiMg(AlH_4)_3$ without considering the weight of LiCl is shown in Figure 2 (a), curve (B). We have found that the TPD curve corresponding to 8 mol% HGNF admixed $LiMg(AlH_4)_3$ sample (Figure 2(a), curve (D)) shows an enhanced desorption kinetics than that of PGNF admixed $LiMg(AlH_4)_3$ (Figure 2(a), curve (C)) but with a loss in hydrogen capacity of ~4 wt.%. This suggests that the $LiMg(AlH_4)_3$ phase decomposes and liberates hydrogen during HGNF admixing through ball-milling.

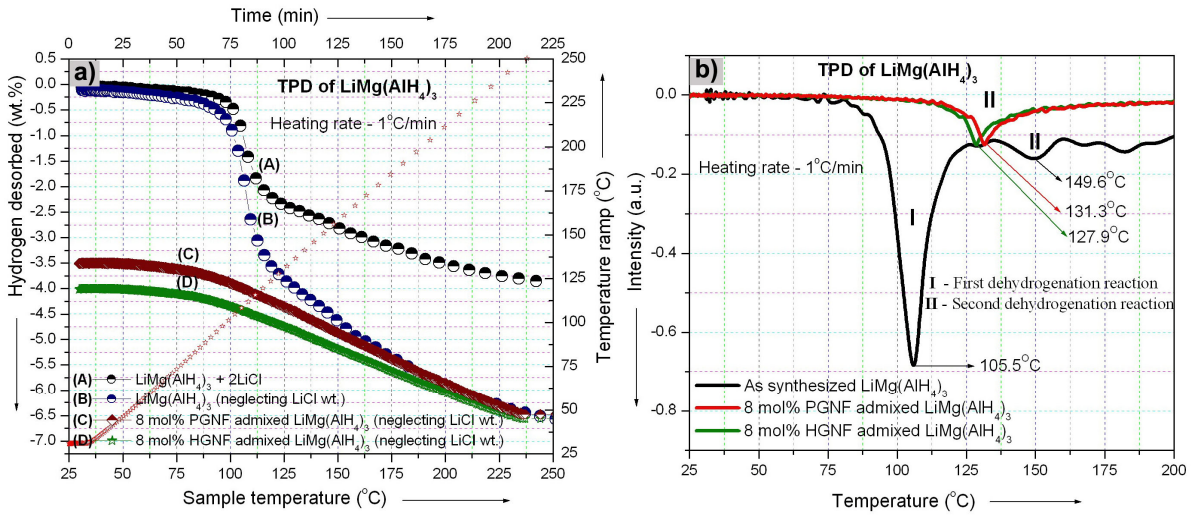

Figure 2: Temperature Programmed Desorption (TPD) a) with respect to hydrogen desorbed (doted curve represents the temperature ramp profile) and b) with respect to peak desorption temperature.

Table 1: Difference between HGNF and PGNF used as catalyst.

Types of GNFs	Catalyst used for synthesis	Surface area (m^2/g)	Average diameter (nm)
Helical GNF (HGNF)	Faceted Ni nanoparticle	125	150
Planar GNF (PGNF)	Spherical Ni nanoparticle	109	200

Representative TEM micrographs of HGNF and PGNF are shown in Figures 3(a) and 3(b).

In order to find the catalytic effect of HGNF in decreasing the activation energy of $LiMg(AlH_4)_3$, we proceed to evaluate this energy from the Arrhenius plot, as described by Janot et al. [11].

The activation energy of desorption process is estimated by plotting the maximum reaction rate (k) as a function of the temperature (T). The reaction rates are obtained from the slopes of the tangents at the inflection points of desorption kinetic curves.

The maximum reaction rates (k) of Eq. (2) at different temperature were calculated from desorption kinetic curves as shown in Figure 4(a). Since the inclusion of LiCl mass in the

kinetic measurement of $LiMg(AlH_4)_3$ affects the rate constant value, we have not considered the weight of LiCl for desorption kinetic measurements.

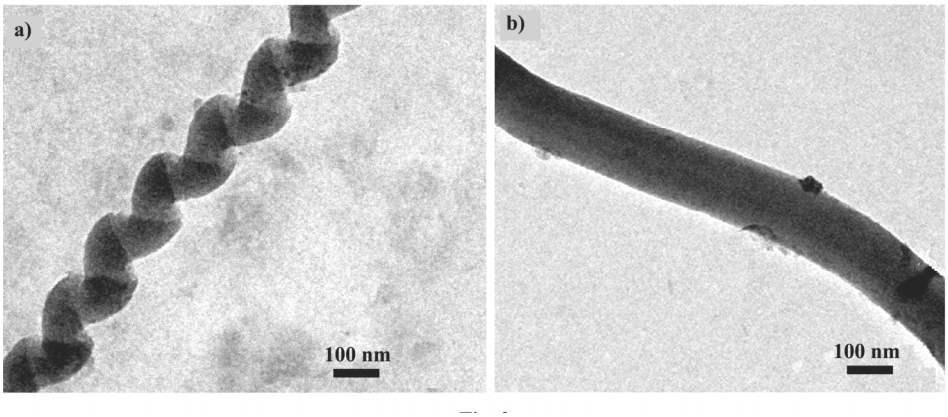

Figure 3: TEM micrograph of GNF a) helical morphology GNF (HGNF) and b) planar morphology GNF (PGNF) (difference between HGNFs and PGNFs are given in table 1).

Quantitative estimation of kinetic barrier was then carried out by the determination of the activation energy (*Ea*) from the well known Arrhenius equation of the form

$$\ln(k) = -Ea/RT + \ln(A) \quad (5)$$

By plotting ln *k* versus *1/T*, *Ea* can be extracted from the linear slope. Figure 4(b) shows the Arrhenius plot for the first-step dehydrogenation of $LiMg(AlH_4)_3$. A good linearity between ln *k* and 1/*T* is obtained with R^2 = 0.99. The activation energy (*Ea*) as calculated corresponds to ~66 kJ/mol.

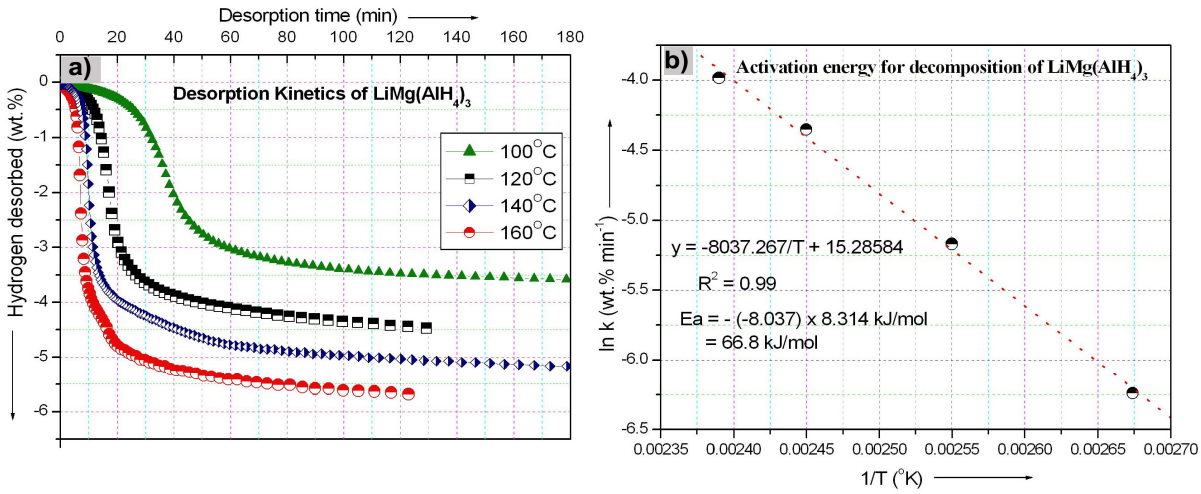

Figure 4: a). desorption kinetic curve of $LiMg(AlH_4)_3$ at different temperatures b) plot of ln *k* vs 1/T for $LiMg(AlH_4)_3$.

3.2 Lithium alanate

In general, $LiAlH_4$ has three-stage decomposition, as represented by the following equations:

$$3LiAlH_4 \rightarrow Li_3AlH_6 + 2Al + 3H_2 \quad (\sim 150°C) \quad (6)$$

$$Li_3AlH_6 \rightarrow 3LiH + Al + 3/2H_2 \quad (\sim 180°C) \quad (7)$$

$$3LiH + 3Al \rightarrow 3LiAl + 3/2H_2 \quad (>400°C) \quad (8)$$

Eq. (6) approximately releases 5.3 wt.% hydrogen and eq. (7) and eq. (8) both release approximately 2.6 wt.% H_2 each. However, eq. (8) is generally not considered usable because it involves very high temperature for decomposition [12].

The catalyst admixing was carried out through ball-milling for 15 min, using the same ballmiller as mentioned above. The optimum molar concentration of GNFs for $LiAlH_4$ has been found to be 8 mol%. Lower concentration of GNF does not produce enhancement in kinetics similar to that from 8 mol% and increasing the molar concentration of GNFs further leads to the decrease in hydrogen storage capacity. For comparison, the dehydrogenation behavior of one hour ball-milled $LiAlH_4$ is also compared with 8 mol% HGNF admixed $LiAlH_4$ sample. Figures 5(a) and 5(b) show representative TPD profile of $LiAlH_4$ sample. There is a loss of ~2 wt.% H_2 in the 8 mol% GNFs admixed $LiAlH_4$ sample, this was estimated by comparing the TPD profile of the ball-milled and pristine $LiAlH_4$.

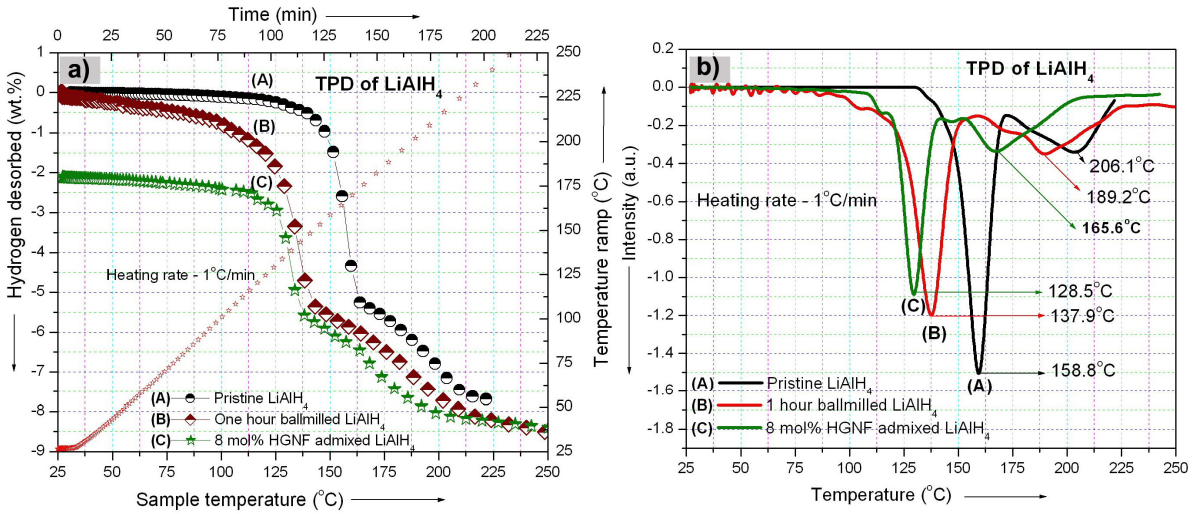

Figure 5: Temperature programmed desorption (TPD) of $LiAlH_4$ a) with respect to hydrogen desorbed (doted curve represents the temperature ramp profile) and b) with respect to peak desorption temperature.

A noticeable feature shown in Figure 5(b) is that for the heating rate of 1ºC/min, the peak desorption temperature for 8 mol% HGNF admixed $LiAlH_4$ sample corresponds to Eq. (6) has been lowered from 158.8°C to 128.5°C and as that for reaction corresponding to Eq. (7) has been lowered from 206.1°C to 165.5°C. It may be mentioned that the effect of increase in the interface area which will result due to ball-milling, will not be able to explain the significant decrease in desorption temperature. Apparently it is the catalytic effect of GNF which leads

to decrease of desorption temperature. The exact role of GNF in improving the dehydrogenation behavior of complex hydride is exactly not known. Based on the known results on the catalytic effect of carbon nanostructures in complex hydrides, it is believed that higher the curvature of catalyst, higher is the catalytic activity. The carbon nanostructures as for example fullerenes have higher curvature than CNTs or graphenes. Hence fullerene has higher catalytic activity [3]. In contrast to PGNF, HGNF has curved surface. Therefore it will have higher catalytic activity than PGNF.

When admixing 8 mol% HGNF with $LiAlH_4$, desorption kinetics of $LiAlH_4$ gets significantly improved. The effect of HGNFs on $LiAlH_4$ is estimated from the activation energy value (*Ea*) calculated for pristine $LiAlH_4$ and 8 mol% HGNF admixed with $LiAlH_4$. In order to find the activation energy of pristine $LiAlH_4$ using Arrhenius relation, the desorption kinetics of pristine $LiAlH_4$ at different temperatures was evaluated. A representative desorption kinetics plot of pristine $LiAlH_4$ at different temperatures and its ln *k* vs *1/T* plot is shown in Figures 6(a) and 6(b), respectively. A good linearity between ln *k* and 1/*T* is obtained with R^2 = 0.99. The activation energy calculated for pristine $LiAlH_4$ is 107 kJ/mol. This value is comparable to the recently reported value of 102 kJ/mol by Blanchard et al.[13].

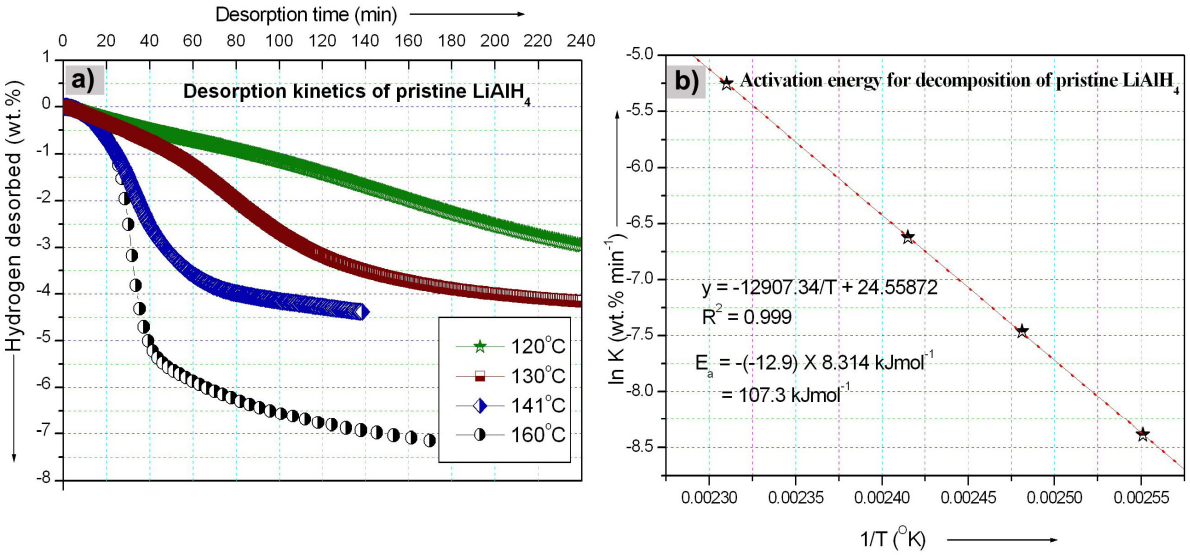

Figure 6: a) dehydrogenation kinetics of pristine $LiAlH_4$ at different temperatures b) plot of ln *k* vs 1/T for calculation of activation energy for reaction correspond to Eq. (5).

The activation energy (*Ea*) calculated for 8 mol% HGNF admixed $LiAlH_4$ is ~68 kJ/mol. This is slightly higher (~16 kJ/mol) than the reported activation energy value (42.6 kJ/mol) of $LiAlH_4$ with transition metal based catalysts (Chen et al, ref [14]). However, there exist some controversial results regarding the activation energy for $LiAlH_4$. For 2 mol% TiC_3.1/3($AlCl_3$) catalyzed $LiAlH_4$, the activation energy calculated by Blanchard et al. [13] is 90 kJ/mol, which is much higher than the estimate value of 42.6 kJ/mol, reported by Chen et al [14]. The dehydrogenation kinetics of 8 mol% HGNF admixed $LiAlH_4$ at different temperatures and its ln *k* vs *1/T* plot is shown in Figures 7(a) and 7(b), respectively.

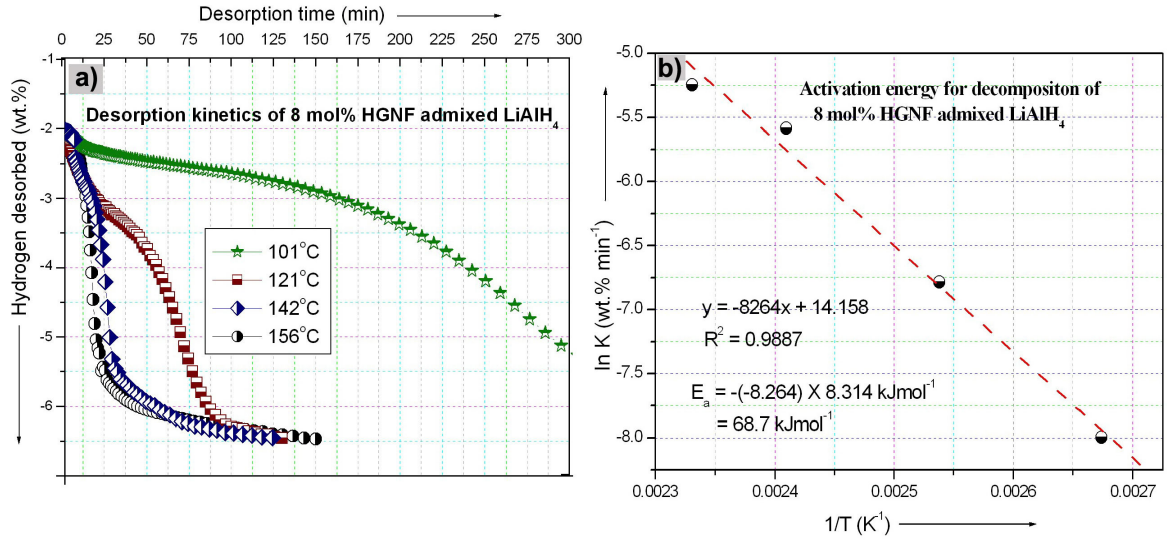

Figure 7: a) dehydrogenation kinetics of 8 mol% HGNF admixed $LiAlH_4$ at various temperatures b) plot of ln *k* vs 1/T for 8 mol% HGNF admixed $LiAlH_4$.

Thus the admixing of 8 mol% HGNF helps to decrease the activation energy for the decomposition of $LiAlH_4$ by 36% (for pristine $LiAlH_4$ calculated *Ea* is 107 kJ/mol, and for 8 mol% HGNF admixed $LiAlH_4$, it is ~68 kJ/mol.

4 Conclusions

The catalytic effect of graphitic nanofibres on $LiMg(AlH_4)_3$ and $LiAlH_4$ has been studied. The dehydrogenation behavior of the samples was studied through TPD and desorption kinetic measurements. We have found that helical morphology of GNF improves the dehydrogenation behavior of both $LiMg(AlH_4)_3$ and $LiAlH_4$. The lowering of desorption temperature for HGNF admixed $LiMg(AlH_4)_3$ as compared to its pristine phase is from 105°C to ~70°C. Whereas the lowering of desorption temperature of HGNF admixed $LiAlH_4$ as compared to pristine $LiAlH_4$ phase is from 159°C to 128°C. However, the decomposition rate of $LiMg(AlH_4)_3$ in the presence of HGNF is higher than that for $LiAlH_4$. The activation energy calculated for the first step decomposition of HGNF admixed $LiAlH_4$ is ~68 $kJmol^{-1}$, whereas that for pristine $LiAlH_4$, it is ~107 kJ/mol. The activation energy calculated for as synthesized $LiMg(AlH_4)_3$ is ~66 kJ/mol. Since the first step decomposition of $LiMg(AlH_4)_3$ occurs during GNF admixing, the activation energy for initial decomposition of GNF admixed $LiMg(AlH_4)_3$ could not be estimated.

Acknowledgement

The authors would like to thank Prof. T.N. Veziroglu, Prof. C.N.R. Rao, Prof. S.K. Joshi, Prof. S.P. Thyagarajan and Prof. D.P. Singh (VC:BHU) for their encouragement and support. Financial support from the Ministry of New and Renewable Energy, the University Grants Commission, DST: Nano Science Technology Unit (BHU) and the Council of Scientific and Industrial Research are thankfully acknowledged.

References

[1] Bogdanovic B, Schwickardi M. Ti-doped alkali metal aluminium hydrides as potential novel reversible hydrogen storage materials. J. Alloys Compd. 1997;253-254:1-9.

[2] Srinivasan S, Escobar D, Goswami Y, Stefanakos E. Effects of catalysts doping on the thermal decomposition behavior of $Zn(BH_4)_2$. Int. J Hydrogen Energy. 2008;33:2268 - 72.

[3] Berseth PA, Harter AG, Zidan R, Blomqvist A, Araujo CM, Scheicher RH, Ahuja R, Jena P. Carbon Nanomaterials as Catalysts for Hydrogen Uptake and Release in $NaAlH_4$. Nano Lett. 2009;9:1501-05.

[4] Serp P, Corrias M, Kalck P. Carbon nanotubes and nanofibers in catalysis. Applied Catalysis A: General. 2003;253:337-58.

[5] Kumar LH, Viswanathan B, Murthy SS. Dehydriding behaviour of $LiAlH_4$-the catalytic role of carbon nanofibres. Int. J Hydrogen Energy. 2008;33:366-73.

[6] Lillo-Rodenas MA, Guo ZX, Aguey-Zinsou KF, Cazorla-Amoros D, Linares-Solano A. Effects of different carbon materials on MgH_2 decomposition. Carbon 2008;46:126-37.

[7] Park C, Baker RTK. Catalytic Behavior of Graphite Nanofiber Supported Nickel Particles. 2. The Influence of the Nanofiber Structure. J. Phys. Chem. B 1998;102:5168-77.

[8] Blank VD, Alshevskiy YL, Zaitsev AI, Kazennov NV, Perezhogin IA, Kulnitskiy BA. Structure and phase composition of a catalyst for carbon nanofiber formation. Scripta Mat. 2006;55:1035-38.

[9] Tang X, Opalka SM, Laube BL, Wu FJ, Strickler JR, Anton DL. Hydrogen storage properties of Na–Li–Mg–Al–H complex hydrides. J. Alloys Compd. 2007;446-447:228-31.

[10] Hudson MSL, Pukazhselvan D, Sheeja GI, Srivastava ON. Studies on synthesis and dehydrogenation behavior of magnesium alanate and magnesium–sodium alanate mixture. Int. J Hydrogen Energy. 2007;32:4933-38.

[11] Janot R, Eymery JB, Tarascon JM. Investigation of the processes for reversible hydrogen storage in the Li–Mg–N–H system. Journal of Power Sources. 2007;164:496-502.

[12] Vittetoe AW, Niemann MU, Srinivasan SS, McGrath K, Kumar A, Goswami DY, Stefanakos EK, Thomas S. Destabilization of $LiAlH_4$ by nanocrystalline MgH_2. Int. J Hydrogen Energy. 2009;34:2333-39.

[13] Blanchard D, Brinks HW, Hauback BC, Norby P, Muller J. Isothermal decomposition of $LiAlD_4$ with and without additives. J. Alloys Compd. 2005;404-406:743-47.

[14] Chen J, Kuriyama N, Xu Q, Takeshita HT, Sakai T. Reversible Hydrogen Storage via Titanium-Catalyzed $LiAlH_4$ and Li_3AlH_6. J. Phys. Chem. B. 2001;105:11214-20.